



Article

A Sustainable and Low-Cost Route to Design NiFe₂O₄ Nanoparticles/Biomass-Based Carbon Fibers with Broadband Microwave Absorption

Wanxi Li * , Fang Guo, Yali Zhao and Yanyun Liu

Department of Materials Science and Engineering, Jinzhong University, Jinzhong 030619, China

* Correspondence: liwanxi1986@163.com

Abstract: Carbon-based microwave-absorbing materials with a low cost, simple preparation process, and excellent microwave absorption performance have important application value. In this paper, biomass-based carbon fibers were prepared using cotton fiber, hemp fiber, and bamboo fiber as carbon sources. Then, the precise loading of NiFe₂O₄ nanoparticles on biomass-based carbon fibers with the loading amount in a wide range was successfully realized through a sustainable and low-cost route. The effects of the composition and structure of NiFe₂O₄/biomass-based carbon fibers on electromagnetic parameters and electromagnetic absorption properties were systematically studied. The results show that the impedance matching is optimized, and the microwave absorption performance is improved after loading NiFe₂O₄ nanoparticles on biomass-based carbon fibers. In particular, when the weight percentage of NiFe₂O₄ nanoparticles in NiFe₂O₄/carbonized cotton fibers is 42.3%, the effective bandwidth of NiFe₂O₄/carbonized cotton fibers can reach 6.5 GHz with a minimum reflection loss of −45.3 dB. The enhancement of microwave absorption performance is mainly attributed to the appropriate electromagnetic parameters with the ϵ' ranging from 9.2 to 4.8, and the balance of impedance matching and electromagnetic loss. Given the simple synthesis method, low cost, high output, and excellent microwave absorption performance, the NiFe₂O₄/biomass-based carbon fibers have broad application prospects as an economic and broadband microwave absorbent.



Citation: Li, W.; Guo, F.; Zhao, Y.; Liu, Y. A Sustainable and Low-Cost Route to Design NiFe₂O₄ Nanoparticles/Biomass-Based Carbon Fibers with Broadband Microwave Absorption. *Nanomaterials* **2022**, *12*, 4063. <https://doi.org/10.3390/nano12224063>

Academic Editors: Lyudmila M Bronstein and Yu L. Raikher

Received: 16 October 2022

Accepted: 14 November 2022

Published: 18 November 2022

Publisher's Note: MDPI stays neutral with regard to jurisdictional claims in published maps and institutional affiliations.



Copyright: © 2022 by the authors. Licensee MDPI, Basel, Switzerland. This article is an open access article distributed under the terms and conditions of the Creative Commons Attribution (CC BY) license (<https://creativecommons.org/licenses/by/4.0/>).

Keywords: biomass-based carbon fibers; NiFe₂O₄ nanoparticles; electromagnetic parameters; microwave absorption performance

1. Introduction

With the widespread application of electronic and electrical equipment, wireless communication systems, and radar stealth technology, the problems of electromagnetic pollution and electromagnetic interference have become increasingly serious, leading to the research on electromagnetic wave-absorbing materials receiving increasing attention [1–3]. Microwave-absorbing materials are being widely applied in both civil and military areas, and the requirements for the material preparation with low cost, high output, and ease to manufacture, and for the performance with thin thickness, lightweight, wide frequency band, and strong absorption are also higher and higher, which brings more challenges to researchers in material preparation and regulation [4–7]. According to the electromagnetic energy conversion principle, to achieve efficient and broadband absorption of electromagnetic waves, microwave-absorbing materials need to have two conditions: one is the electromagnetic waves can effectively enter the interior of microwave-absorbing materials, which involves the problem of impedance matching; the other is the absorbing material can effectively attenuate the electromagnetic waves entering its interior, which involves the issue of electromagnetic loss [8,9]. Impedance matching and electromagnetic loss are usually contradictory, and the controllable adjustment of electromagnetic parameters plays a decisive role in balancing impedance matching and electromagnetic loss [10–12].

In recent years, carbon materials have attracted extensive attention from microwave-absorbing material researchers because of their good chemical and thermal stability, excellent dielectric properties, and low density [13,14]. Optimizing the composite consisting of magnetic nanomaterial and carbon material can not only overcome the defect of the high density of magnetic materials such as ferrite, magnetic metal, magnetic metal oxide, and alloy, but also regulate electromagnetic parameters and improve electromagnetic matching, achieving better electromagnetic wave absorption than a single microwave-absorbing material. Various carbon materials, such as carbon fibers, carbon nanotubes, graphene, and metal organic-framework compounds have been widely used as carbon sources of carbon-based composite microwave-absorbing materials [15–18]. Biomass is a cheap, eco-friendly, and resource-rich renewable resource. After the carbonization of biomass, porous carbon materials with multi-stage pore size distribution can be obtained [19,20]. Recent studies have found that the porous carbon structure can not only reduce the density of materials, but also enhance impedance matching and achieve excellent microwave absorption performance [21,22]. Zhou et al. [23] prepared three-dimensional porous carbon/Fe₃O₄@Fe at different calcination temperatures using a towel gourd sponge as carbon source. When the calcination temperature was 600 °C, the minimum reflection loss (RL) of the composite was −49.6 dB with an effective bandwidth of 5 GHz. The synergistic effects of three-dimensional porous structure, interface polarization, dielectric loss, and magnetic loss contribute to the enhancement of microwave absorption performance. Therefore, it is a sustainable, ubiquitous, and low-cost method to obtain porous carbon materials from biomass. Because of the unique characteristics, such as hierarchical structure, periodic mode, and some individual nanostructures, it is desirable to prepare porous carbon microwave absorbent using biomass under mild conditions. Although some progress has been made in the exploration of such materials, the proportion regulation of porous carbon materials and magnetic components is the basis and key for the continuous and controllable regulation of electromagnetic parameters, which requires breakthroughs in the selection of carbon sources, the choice of preparation methods, and the control of process conditions.

Some previous results, both for conductive and magnetic inclusions, showed the influence of the shape of the additives in the electromagnetic behavior of the composites. Pinto et al. showed how additives based on magnetic metallic iron with the same crystallographic structure but with different morphologies (filaments and spherical particles) confer different electromagnetic characteristics [24]. Other works, such as Copper microwires composite and Fe-based amorphous magnetic microwires with a high aspect relationship allowed the obtention of sheets of thickness below 1 mm with reflection loss below −20 dB in the X-band [25,26]. Natural plant fiber materials have orderly optimized and stable morphology and structure. Moreover, the main component of natural plant fiber is cellulose, which is an economical and feasible raw material for the preparation of porous carbon fibers with multi-level pore size distribution. At present, the research of natural plant fibers in the field of microwave-absorbing materials has just started [27–29]. Ferrite nanoparticles have high permeability and good oxidation resistance. The electromagnetic parameters of carbon matrix composites can be continuously adjusted by regulating the loading amount of ferrite nanoparticles [30,31]. This feature can not only overcome the shortcomings of easy agglomeration and high density of magnetic materials, but also facilitate the study of electromagnetic loss mechanism and broaden the frequency band of microwave absorbents.

In this paper, we take the carbonized cotton fiber, carbonized hemp fiber, and carbonized bamboo fiber obtained by calcination of cotton fiber, hemp fiber, and bamboo fiber as carbon sources, and introduce different contents of NiFe₂O₄ nanoparticles, preparing a new carbon-based microwave-absorbing material with excellent microwave absorption performance by continuously adjusting electromagnetic parameters through composition design. The effects of the composition and structure of NiFe₂O₄ nanoparticles/biomass-based carbon fibers on electromagnetic parameters and microwave absorption properties were systematically investigated. The electromagnetic loss mechanism was also revealed, which

provided theoretical support and experimental basis for designing cheap, lightweight, and efficient carbon-based microwave-absorbing materials.

2. Materials and Methods

2.1. Materials

Ferric chloride ($\text{FeCl}_3 \cdot 6\text{H}_2\text{O}$), nickel nitrate ($\text{Ni}(\text{NO}_3)_2 \cdot 6\text{H}_2\text{O}$), and sodium hydroxide (NaOH) are analytical reagent grade, which were purchased from Shanghai Macklin Biochemical Co., Ltd. (Shanghai, China), Tianjin Bodi Chemical Co., Ltd. (Tianjin, China), and Tianjin Kaitong Chemical Reagent Co., Ltd. (Tianjin, China), respectively. The natural plant fibers were purchased from Jiangxi Zhonggan Medical Instrument Co., Ltd. (Nanchang, China). High purity N_2 (Taiyuan Taineng Gas Co., Ltd., Taiyuan, China) was used as protective gas.

2.2. Preparation of NiFe_2O_4 /Carbonized Cotton Fibers

NiFe_2O_4 /carbonized cotton fibers were fabricated through a three-step process.

(1) An appropriate amount of cotton fibers were put into a porcelain boat, then calcinated at $700\text{ }^\circ\text{C}$ for 3 h in a tubular electric furnace in a N_2 atmosphere. The sample obtained was carbonized cotton fiber, named CCF.

(2) Amounts of 0.01 mol $\text{FeCl}_3 \cdot 6\text{H}_2\text{O}$ and 0.005 mol $\text{Ni}(\text{NO}_3)_2 \cdot 6\text{H}_2\text{O}$ were dissolved in 30 mL water, and then 30 mL NaOH solution with the concentration of 2 mol/L was added under constant stirring. After stirring for 0.5 h, the precursor was put into a hydrothermal reactor and heated, at $200\text{ }^\circ\text{C}$, for 15 h in an electric blast drying oven. After cooling, washing, and drying at $60\text{ }^\circ\text{C}$ for 12 h, NiFe_2O_4 nanoparticles were prepared.

(3) First, 0.3 g, 0.5 g, 1.0 g, and 1.5 g of NiFe_2O_4 nanoparticles were put into a beaker with 30 mL distilled water, respectively, and ultrasonic for 0.5 h in an ultrasonic cleaner to form NiFe_2O_4 suspension. Then, a certain quality of carbonized cotton fibers were put into the beaker and ultrasonicated for 1 h. Finally, the carbonized cotton fibers were taken out by tweezers, and dried at $60\text{ }^\circ\text{C}$ for 6 h. Different contents of NiFe_2O_4 nanoparticles were loaded on the carbonized cotton fibers, and the obtained samples were named NiFe_2O_4 /CCF-1, NiFe_2O_4 /CCF-2, NiFe_2O_4 /CCF-3, and NiFe_2O_4 /CCF-4, respectively.

2.3. Preparation of NiFe_2O_4 /Carbonized Hemp Fibers and NiFe_2O_4 /Carbonized Bamboo Fibers

Carbonized hemp fibers and carbonized bamboo fibers were prepared by changing the cotton fibers to hemp and bamboo fibers under the same conditions. NiFe_2O_4 /carbonized hemp fibers and NiFe_2O_4 /carbonized bamboo fibers were designed with the same preparation method of NiFe_2O_4 /CCF-2, which were named NiFe_2O_4 /CHF and NiFe_2O_4 /CBF, respectively.

2.4. Characterization

XRD-6100 powder X-ray diffractometer (XRD, Shimadzu, Kyoto, Japan) was used to analyze the phase composition of the samples. The morphology of the samples was characterized by a JSM-7001F scanning electron microscope (SEM, Japan Electronics Co., Ltd., Kyoto, Japan) with energy dispersive spectrometer (EDS, Bruker, Karlsruhe, Germany) and a JEM-1011 transmission electron microscope (TEM, Japan Electronics Co., Ltd., Kyoto, Japan). STA6000 synchronous thermal analyzer (PerkinElmer, Waltham, MA, USA) was used for thermogravimetric (TG) analysis, and the temperature ranged from room temperature to $700\text{ }^\circ\text{C}$, with a heating rate of $10\text{ }^\circ\text{C}/\text{min}$. The magnetic properties of the samples were studied by using a Lakeshore 7404 vibrating sample magnetometer (VSM, LakeShore Company, Columbus, OH, USA). For the microwave absorption performance test, the synthetic product was mixed with paraffin and pressed into a cylindrical compact ($\Phi_{\text{out}} = 7.0\text{ mm}$, $\Phi_{\text{in}} = 3.0\text{ mm}$). Then, the annular test sample in the coaxial mold was connected with an Agilent N5244A vector network analyzer (Agilent Technologies Inc., Santa Clara, CA, USA) to test the scattering parameters (abbreviated as S parameters, including S11, S21, S12, and S22). The complex permittivity (ϵ_r) and the complex permeability (μ_r) of the sample were calculated based on the S parameters in the vector network

analyzer in the frequency range of 2–18 GHz. Based on the above-measured ϵ_r and μ_r , the transmission line theory was used to calculate the RL, which could be calculated by the following formulas: [32,33]

$$Z_{in} = (\mu_r/\epsilon_r)^{1/2} \tanh[j(2\pi f d/c)(\mu_r \epsilon_r)^{1/2}], \quad (1)$$

$$RL(\text{dB}) = 20 \log |(Z_{in} - Z_0)/(Z_{in} + Z_0)|, \quad (2)$$

where Z_{in} is the input impedance of the absorbent, Z_0 is the characteristic impedance of the free space, f is the frequency of the electromagnetic wave, d is the thickness of the absorbent, and c is the speed of light in free space.

3. Results

XRD was used to analyze the phase of the samples. Figure 1 shows the XRD spectra of CCF, NiFe₂O₄/CCF-1, NiFe₂O₄/CCF-2, NiFe₂O₄/CCF-3, and NiFe₂O₄/CCF-4. For CCF, wide peaks at approximately 10°–30° and 40–50° indicate amorphous carbon [34]. For NiFe₂O₄/CCF-1, NiFe₂O₄/CCF-2, NiFe₂O₄/CCF-3, and NiFe₂O₄/CCF-4, apart from the diffraction peaks of amorphous carbon, all diffraction peaks correspond to the NiFe₂O₄ spinel phase (JCPDS NO.10-0325). The sharp diffraction peaks indicate the good crystallinity of NiFe₂O₄. From NiFe₂O₄/CCF-1 to NiFe₂O₄/CCF-4, the diffraction peaks of NiFe₂O₄ gradually increase, and the amorphous carbon peaks gradually weaken, indicating the increase in the loading amount of NiFe₂O₄. These results show that the coexistence of NiFe₂O₄ and amorphous carbon can be achieved by this method. In addition, the XRD patterns have no impurity peak, indicating the high purity of NiFe₂O₄ nanoparticles.

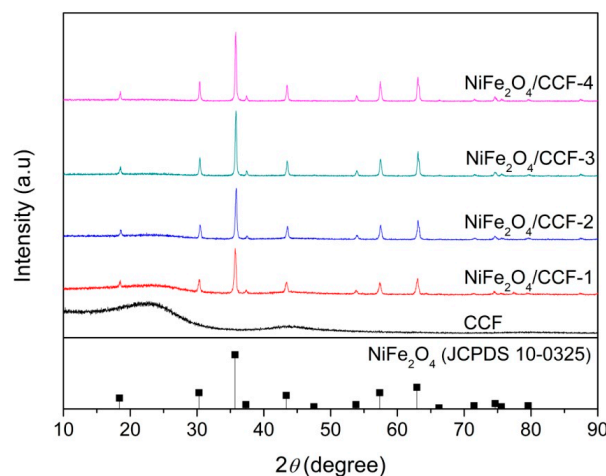


Figure 1. XRD patterns of CCF, NiFe₂O₄/CCF-1, NiFe₂O₄/CCF-2, NiFe₂O₄/CCF-3, and NiFe₂O₄/CCF-4.

The morphology of the synthetic samples was studied by SEM, as shown in Figure 2. Figure 2a,b shows the SEM images of CCF, and it is clear that the CCF is twisted and fibrous with a smooth fiber surface. Figure 2c–i shows the SEM images of NiFe₂O₄/CCF-1, NiFe₂O₄/CCF-2, NiFe₂O₄/CCF-3, and NiFe₂O₄/CCF-4. It is obvious that the NiFe₂O₄ nanoparticles are successfully loaded on CCF. Moreover, the NiFe₂O₄ nanoparticles have octahedral morphology, and the particle size is about 100 nm. From NiFe₂O₄/CCF-1 to NiFe₂O₄/CCF-4, the number of the NiFe₂O₄ nanoparticles on CCF shows an upward trend, indicating the increase in the loading amount of NiFe₂O₄ nanoparticles, which is consistent with the XRD results. The TEM images of the NiFe₂O₄ nanoparticles were shown in Figure S1. It is clear that the NiFe₂O₄ nanoparticles have clear edges and corners, and the size of the vast majority of nanoparticles is in the range of 80–120 nm. Figure 3 shows the EDS element diagram and elemental mapping images of NiFe₂O₄/CCF-2. It displays that the NiFe₂O₄/CCF-2 is mainly composed of C, O, Fe, and Ni elements, and the O, Fe, and Ni elements are displayed along the NiFe₂O₄ nanoparticles.

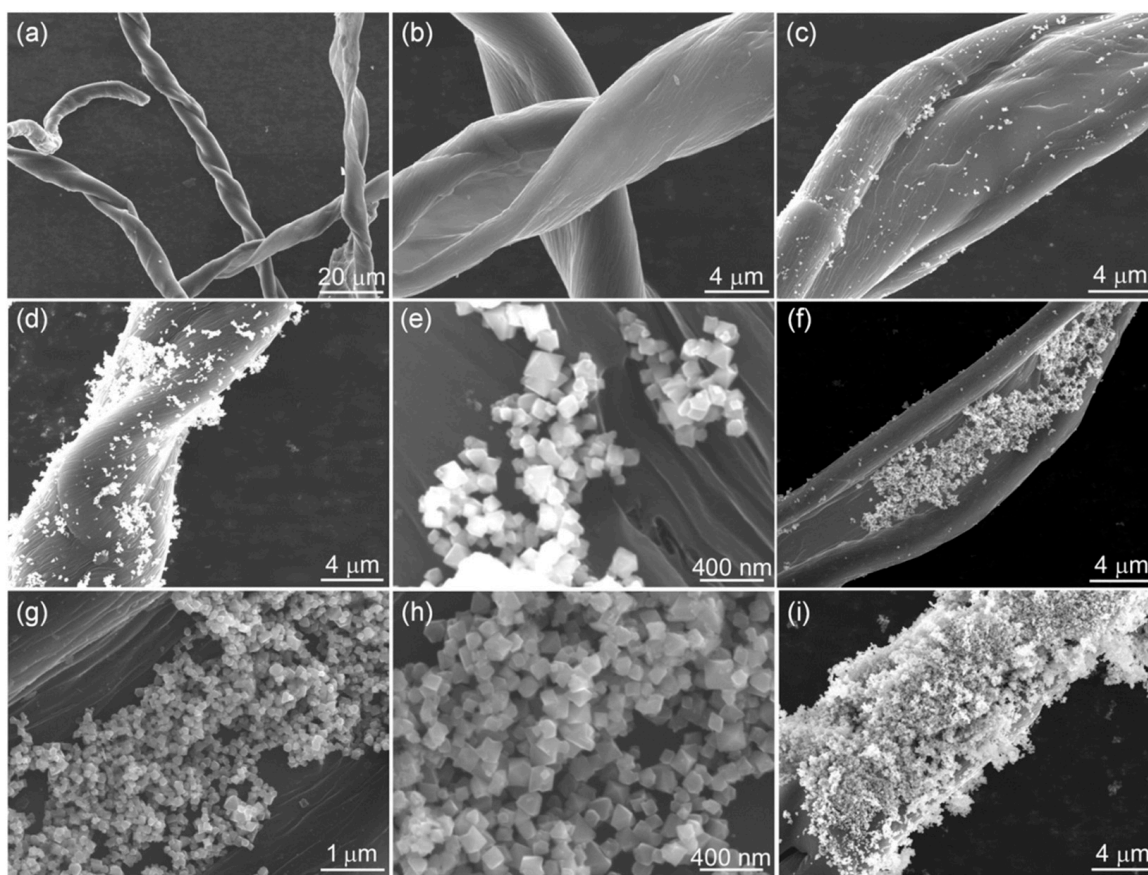


Figure 2. SEM images of the synthesized samples: (a,b) CCF, (c) NiFe₂O₄/CCF-1, (d,e) NiFe₂O₄/CCF-2, (f–h) NiFe₂O₄/CCF-3, and (i) NiFe₂O₄/CCF-4.

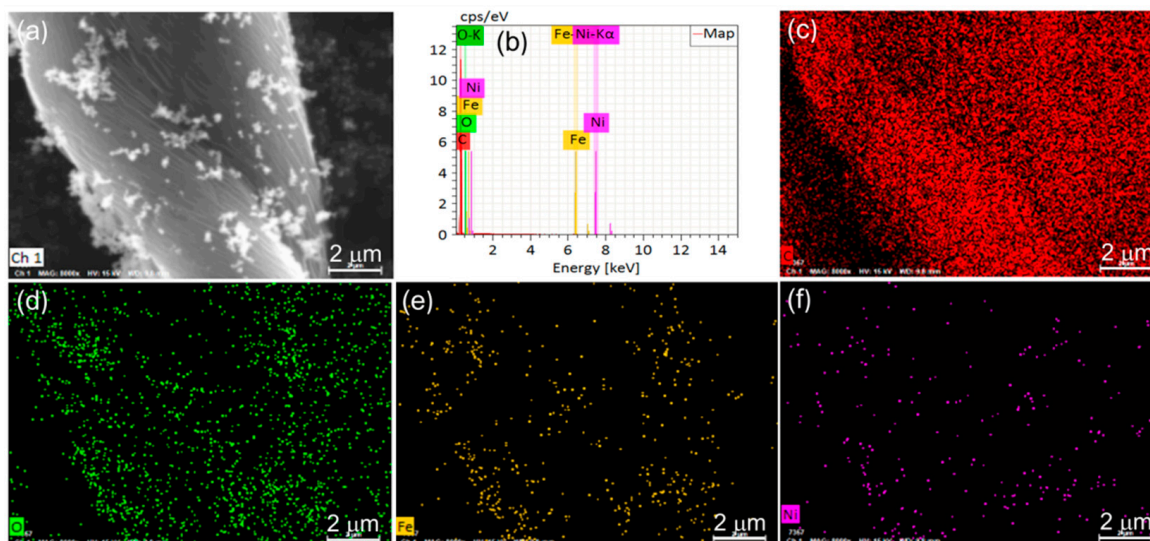


Figure 3. (a) SEM image, (b) EDX spectra, and (c–f) elemental mapping images of NiFe₂O₄/CCF-2.

To quantitatively analyze the loading amount of NiFe₂O₄ nanoparticles on the NiFe₂O₄/carbonized cotton fibers, we studied the TG curves of NiFe₂O₄/carbonized cotton fibers in the air atmosphere, as shown in Figure 4. The TG curves show the mass percentage of the residue in the process of temperature change. Since the carbonized cotton fiber can be burned completely in air atmosphere, and the residual product is only NiFe₂O₄, the loading amount of NiFe₂O₄ nanoparticles can be estimated according to the TG curves. It is estimated that the loading amount of NiFe₂O₄ nanoparticles in NiFe₂O₄/CCF-1,

NiFe₂O₄/CCF-2, NiFe₂O₄/CCF-3, and NiFe₂O₄/CCF-4 is 7.6 wt% (weight percentage), 21.0 wt%, 42.3 wt%, and 55.3 wt%, respectively. In addition, the NiFe₂O₄/carbonized cotton fibers have small weight loss below 450 °C, displaying good thermal stability.

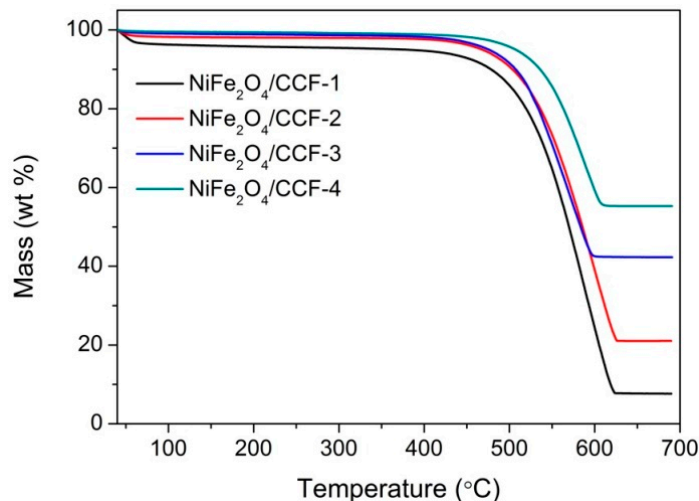


Figure 4. TG curves of NiFe₂O₄/carbonized cotton fibers in air atmosphere.

To study the magnetic properties of NiFe₂O₄/CCF-1, NiFe₂O₄/CCF-2, NiFe₂O₄/CCF-3, and NiFe₂O₄/CCF-4, we measured the hysteresis loops at room temperature within the magnetic field of −20 kOe–20 kOe, as shown in Figure 5. It can be seen that these four samples all show ferromagnetic behavior. The saturation magnetization (M_S) of NiFe₂O₄/CCF-1, NiFe₂O₄/CCF-2, NiFe₂O₄/CCF-3, and NiFe₂O₄/CCF-4 is 4.7 emu/g, 10.5 emu/g, 22.3 emu/g, and 30.3 emu/g, respectively. It is obvious that the M_S increases with the increase in the loading amount of NiFe₂O₄ nanoparticles, and this result is consistent with the XRD, SEM, and TG results.

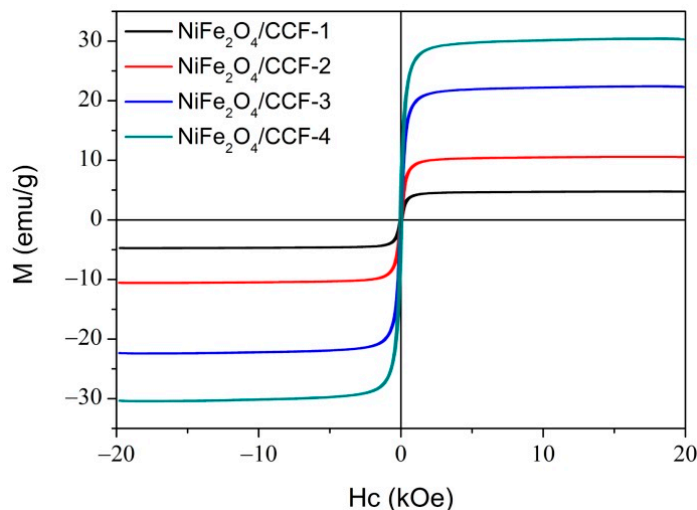


Figure 5. The hysteresis loops of NiFe₂O₄/carbonized cotton fibers.

From the above analysis, NiFe₂O₄/carbonized cotton fibers with different loading amounts of NiFe₂O₄ nanoparticles were successfully prepared. Generally speaking, electromagnetic parameters are the most direct characterization parameters of the interaction between absorbing materials and electromagnetic waves, so the regulation of electromagnetic parameters is the most direct and effective means of designing absorbing materials. The most important electromagnetic parameters are complex permittivity ($\epsilon_r = \epsilon' - j\epsilon''$) and complex permeability ($\mu_r = \mu' - j\mu''$). ϵ' and ϵ'' , respectively, represent the capacity and loss

of electric field energy, while μ' and μ'' , respectively, represent the storage and loss of magnetic energy [35,36]. Figure 6 shows the complex permittivity and complex permeability of CCF, NiFe₂O₄/CCF-1, NiFe₂O₄/CCF-2, NiFe₂O₄/CCF-3, and NiFe₂O₄/CCF-4 with the filling ratio of 25 wt% in paraffin matrix. As can be seen from Figure 6a,b, the ϵ' all show a downward trend in the frequency range of 2–18 GHz. This is a typical frequency dispersion phenomenon, which widely exists in carbon materials and is conducive to microwave absorption [37,38]. In addition, the ϵ' decreases with the increase in NiFe₂O₄ content owing to the poor conductivity of NiFe₂O₄ nanoparticles. This is because the introduction of the NiFe₂O₄ nanoparticles into carbonized cotton fibers hinders the electron migration, resulting in fewer conductive network connections and reduced conductivity of the composite. For NiFe₂O₄/CCF-4, the ϵ'' is stable at about 2.1 in the frequency range of 2–18 GHz, while the ϵ'' slowly decreases from 7.6, 7.4, 4.4, and 3.5 to 5.1, 4.9, 3.4, and 2.4, respectively, for CCF, NiFe₂O₄/CCF-1, NiFe₂O₄/CCF-2, and NiFe₂O₄/CCF-3. According to the Debye theory, the relationship between ϵ' and ϵ'' can be further deduced as the following formula: [39,40].

$$\left(\epsilon' - \frac{\epsilon_s + \epsilon_\infty}{2}\right)^2 + (\epsilon'')^2 = \left(\frac{\epsilon_s - \epsilon_\infty}{2}\right)^2 \quad (3)$$

where ϵ_s and ϵ_∞ are static dielectric constant and dielectric constant at infinite frequency, respectively. Therefore, the Debye relaxation process can be represented by the Cole–Cole semicircle, and a semicircle represents a relaxation process. As shown in Figure S2, the CCF, NiFe₂O₄/CCF-1, NiFe₂O₄/CCF-2, and NiFe₂O₄/CCF-3 display two Cole–Cole semicircles, and the NiFe₂O₄/CCF-4 displays three Cole–Cole semicircles. The distinct Cole–Cole semicircles indicate the occurrence of the polarization relaxation process, and NiFe₂O₄/CCF-4 shows a stronger polarization relaxation behavior. As can be seen from Figure 6c,d, the μ' and μ'' are very low for CCF, showing a weak storage and loss of magnetic energy in the range of 2–18 GHz. Moreover, the μ'' shows three vibration peaks at about 7 GHz, 12 GHz, and 17 GHz, and increases with the increase in NiFe₂O₄ content due to the magnetic properties of NiFe₂O₄ nanoparticles. Generally speaking, the magnetic loss is usually related to natural resonance, exchange resonance, and eddy current loss [41]. Eddy current loss can be determined by C_0 ($C_0 = \mu''\mu'^{-2}f^{-1} = 2\pi\mu_0\sigma d^2/3$) [42,43]. If the main reason for the magnetic loss is eddy current loss, the value of C_0 is constant. The C_0 displays a similar vibration trend to that of μ'' in the frequency range 2–18 GHz (Figure S3), confirming that the natural resonance and exchange resonance are the main magnetic loss mechanism.

Generally speaking, a RL value lower than -10 dB means more than 90% microwave absorption. Only absorbent with RL lower than -10 dB can be used in practice, so the effective bandwidth represents the width of the frequency range when RL = -10 dB. According to the formulas (1) and (2) above, the RL is closely related to the thickness of the absorbent and the frequency of the electromagnetic wave. The minimum RL and effective bandwidth are obtained from the RL curve, so the minimum RL and effective bandwidth of microwave absorption are closely related to the thickness of the absorbent. Therefore, we simulated the RL curves of CCF, NiFe₂O₄/CCF-1, NiFe₂O₄/CCF-2, NiFe₂O₄/CCF-3, and NiFe₂O₄/CCF-4 at different thicknesses, as shown in Figure 7. As can be seen from Figure 7a, for CCF, the effective bandwidth is 4.5 GHz (13.5–18 GHz) at a thickness of 1.5 mm. For NiFe₂O₄/CCF-1, when the thickness is 2 mm, the effective bandwidth is also 4.5 GHz (10.5–15 GHz). For NiFe₂O₄/CCF-2, when the thickness is 2 mm, the effective bandwidth can reach 5.8 GHz (11.7–17.5 GHz). For NiFe₂O₄/CCF-3, when the thickness is 2.5 mm, the effective bandwidth reaches 6.5 GHz (11.3–17.8 GHz) with a minimum RL of -33.2 dB; when the thickness rises to 3 mm, the minimum RL is -45.3 dB. For NiFe₂O₄/CCF-4, the minimum RL is -18.8 dB with an effective bandwidth of 5.6 GHz (11.9–17.5 GHz). In addition, as shown in Figure 7a–e, it can be seen that the RL peak moves to the low-frequency region with increasing thickness. Figure 7f shows the RL curves at 2.5 mm for these five samples. Obviously, the RL peak shifts to the high-frequency region by decreasing the complex permittivity under the same thickness by comparing these five samples, and this can be explained by the geometric

effect [44,45]. When the thickness (t_m) of the absorber follows the 1/4 wavelength model: $t_m = n\lambda_0/4(|\mu_r| |\varepsilon_r|)^{1/2} = nc/4f_m(|\mu_r| |\varepsilon_r|)^{1/2} (n=1,3,5, \dots)$, the input impedance is the same as the air wave impedance, and the RL (dB) reaches a minimum value. Simulation and calculation of the absorber thickness (t_m) versus peak frequency (f_m) for these five samples are shown in Figure S4, and it is obvious that the calculated results agree well with the simulated values. For the 1/4 wavelength model, the f_m is inversely proportional to the t_m and complex permittivity. For the same sample with the same μ_r and ε_r , the f_m is inversely proportional to the t_m , so the RL curve moves to the low frequency with increasing the thickness. For different sample in the same thickness, the RL curve moves to the high frequency with decreasing the electromagnetic parameters. Thus, from CCF to NiFe₂O₄/CCF-4, it is understandable that the optimal RL moves to the high thickness with decreasing the complex permittivity for these five samples. As an essential standard for evaluating microwave absorption performance, the minimum RL value and effective bandwidth are also compared with other reported carbon-based absorbers, as shown in Table 1 [46–53]. Obviously, the NiFe₂O₄/carbonized cotton fibers show wider effective bandwidth and stronger RL with a low filling rate. What is more, compared with the microwave absorbers such as ferrite, magnetic metal, magnetic metal oxide, and alloy, the NiFe₂O₄/CCF has a lower density; compared with the preparation of carbon fiber, the CCF has a very simple preparation method [54]. In a word, the use of cotton fibers, simple preparation methods, and excellent microwave absorption performance give NiFe₂O₄/CCF broad application prospects as an economical, lightweight, and broadband microwave absorber.

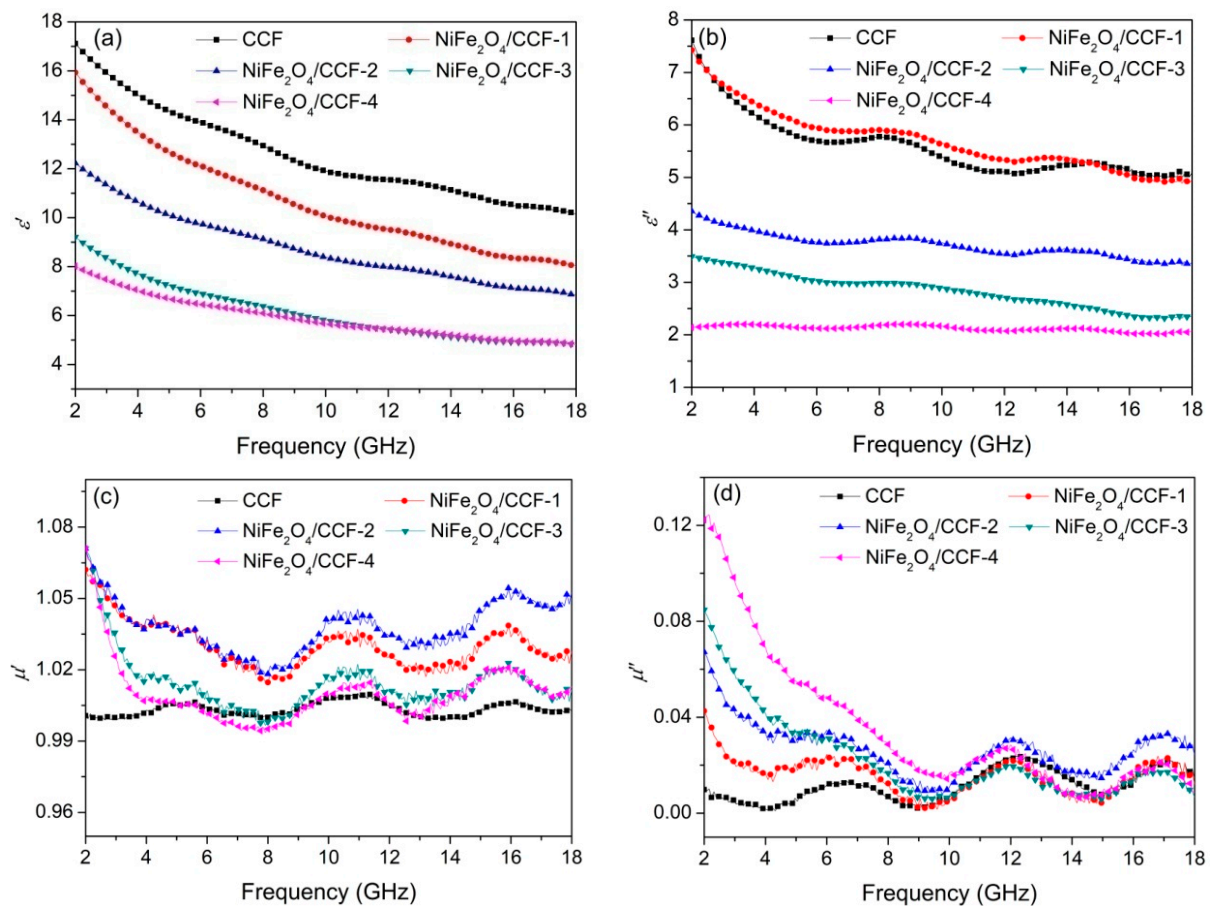


Figure 6. Frequency dependence of (a) ε' , (b) ε'' , (c) μ' , and (d) μ'' for CCF, NiFe₂O₄/CCF-1, NiFe₂O₄/CCF-2, NiFe₂O₄/CCF-3, and NiFe₂O₄/CCF-4.

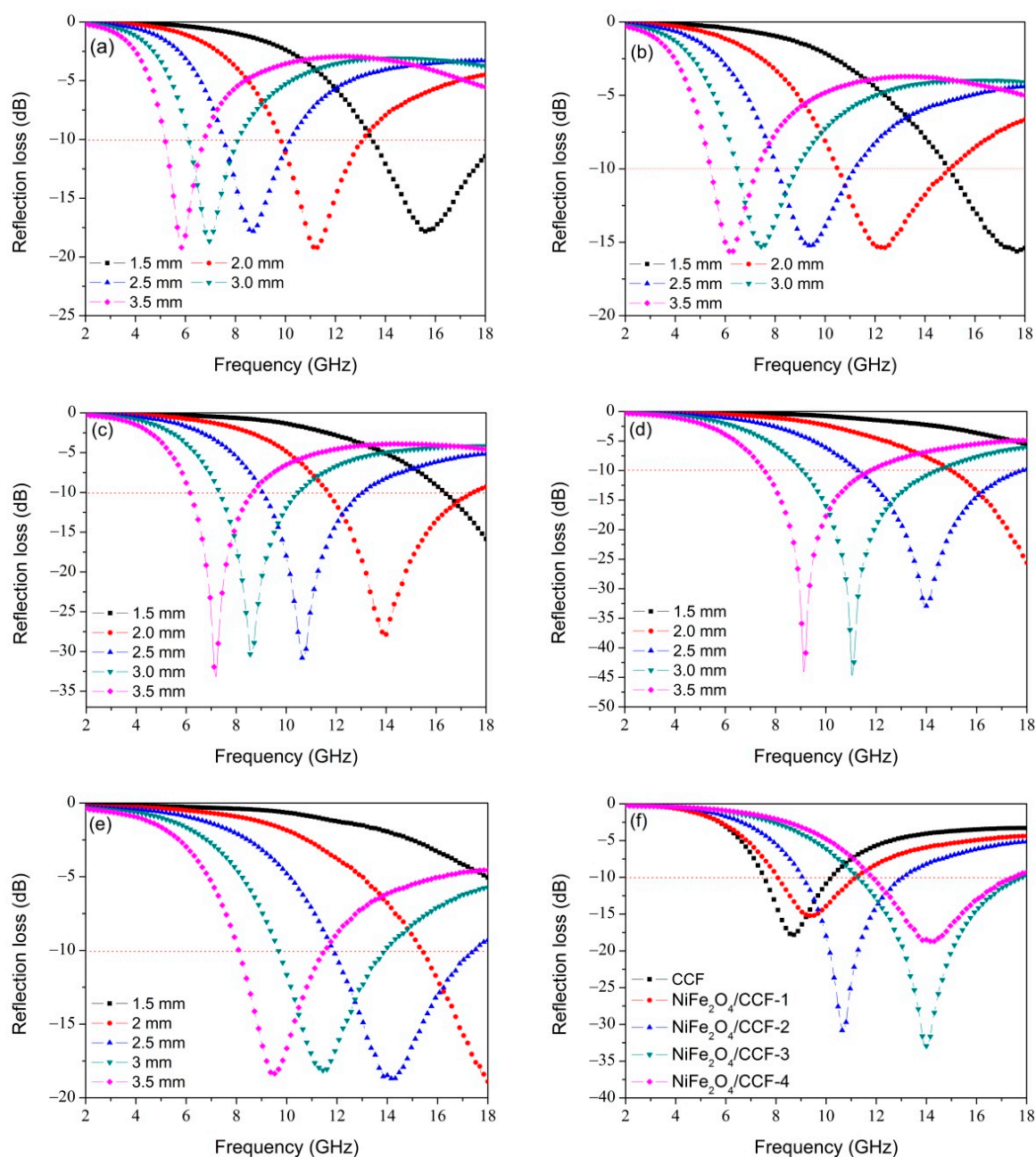


Figure 7. The simulated RL curves of (a) CCF, (b) NiFe₂O₄/CCF-1, (c) NiFe₂O₄/CCF-2, (d) NiFe₂O₄/CCF-3, and (e) NiFe₂O₄/CCF-4 at different thicknesses. (f) RL curves at 2.5 mm thickness for these five samples.

Table 1. Microwave absorption performance of some reported carbon-based absorbents.

Sample	Filling Rate (wt%)	Effective Absorption Bandwidth (GHz)	Minimum RL (dB)	References
MOF-Derived Porous Co/C Nanocomposites	60	5.8	−35.3	[46]
NiFe ₂ O ₄ hollow particle/graphene	15	4.5	−40.9	[47]
Ferrite/Co/porous carbon	70	4.8	−31.0	[48]
Fe@porouscarbon@carbonfiber	25	5.2	−46.2	[49]
RGO-PANI-NiFe ₂ O ₄	30	5.3	−49.7	[50]
Ni/Carbon nanocomposites	25	4.4	−21.2	[51]
CoNi@Ccomposites	50	5.0	−35.8	[52]
CoFe ₂ O ₄ @graphene composites	45	4.6	−42	[53]
NiFe ₂ O ₄ /carbonized cotton fibers	25	6.5	−45.3	This work

Impedance matching and electromagnetic loss are two key factors affecting microwave absorption performance. The impedance matching can be expressed by the impedance matching coefficient ($Z = Z_{in}/Z_0 = (\mu_r/\epsilon_r)^{1/2}$) [55,56]. The closer the Z is to 1, the better the impedance matching is. Recent studies have found that the ϵ_r value is much higher than the μ_r value for carbon materials [57,58]. Therefore, the decrease in the ϵ_r can increase the impedance matching coefficient and improve the impedance matching of the absorbent. Moreover, the electromagnetic loss can be determined by the dielectric loss factor ($\tan\delta_e = \epsilon''/\epsilon'$) and magnetic loss factor ($\tan\delta_m = \mu''/\mu'$) [59,60]. Figure 8 shows the impedance matching coefficient, $\tan\delta_e$, and $\tan\delta_m$ of CCF, NiFe₂O₄/CCF-1, NiFe₂O₄/CCF-2, NiFe₂O₄/CCF-3, and NiFe₂O₄/CCF-4. As seen in Figure 8a, the Z follows the order of CCF < NiFe₂O₄/CCF-1 < NiFe₂O₄/CCF-2 < NiFe₂O₄/CCF-3 < NiFe₂O₄/CCF-4, which is opposite to the complex permittivity. So the existence of NiFe₂O₄ with relatively lower conductivity improves the percolation threshold in the NiFe₂O₄/biomass-based carbon fibers system and hence maintains a good impedance matching [61]. As seen in Figure 8b,c, it is obvious that the $\tan\delta_e$ is much larger than the $\tan\delta_m$, showing that the dielectric loss plays a major role. What is more, the $\tan\delta_e$ shows an upward trend in the frequency of 2–18 GHz, which is highly beneficial to high-frequency microwave absorption. The $\tan\delta_m$ shows a similar tendency to that of μ'' , showing that the magnetic loss is mainly influenced by the imaginary part of the complex permeability. For CCF and NiFe₂O₄/CCF-1, although the $\tan\delta_e$ is higher than 0.4 in the frequency of 2–18 GHz, the impedance matching coefficient is much lower than that of NiFe₂O₄/CCF-3, so the microwave absorption performance is slightly worse. For NiFe₂O₄/CCF-4, although the impedance matching is the best, the electromagnetic loss is relatively small, which is not conducive to microwave absorption. For NiFe₂O₄/CCF-3, the $\tan\delta_e$ is only lower than NiFe₂O₄/CCF-1, while the $\tan\delta_m$ is only lower than NiFe₂O₄/CCF-4, so the NiFe₂O₄/CCF-3 has relatively high electromagnetic loss. In addition, the low value of -45.3 dB at 11 GHz may be attributed to the high $\tan\delta_e$ and $\tan\delta_m$ value in the range of 10–14 GHz. Therefore, the excellent microwave absorption performance of NiFe₂O₄/CCF-3 can be attributed to the appropriate loading amount of NiFe₂O₄ nanoparticles with moderate electromagnetic parameters, and the balance of impedance matching and electromagnetic loss.

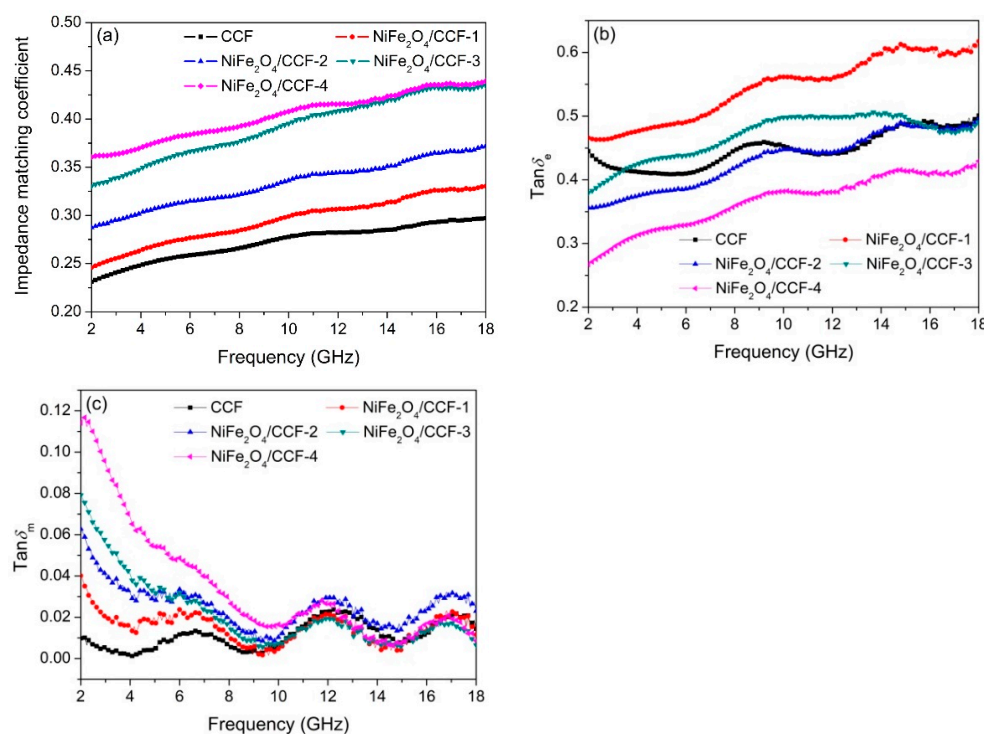


Figure 8. Frequency dependence of (a) impedance matching coefficient, (b) $\tan\delta_e$, and (c) $\tan\delta_m$ of CCF, NiFe₂O₄/CCF-1, NiFe₂O₄/CCF-2, NiFe₂O₄/CCF-3, and NiFe₂O₄/CCF-4.

During the research, NiFe₂O₄/carbonized hemp fibers were also successfully prepared by changing the cotton fibers to hemp fibers under the same conditions. Figure 9a shows the XRD spectrum of NiFe₂O₄/CHF. In addition to the diffraction peaks of NiFe₂O₄, the wide peaks at 10°–30° and 40°–50° are the diffraction peaks of carbonized hemp fibers. Figure 9b shows the TG curves of NiFe₂O₄/CHF in the air atmosphere, revealing that the loading amount of NiFe₂O₄ nanoparticles in NiFe₂O₄/CHF is 8.3 wt%. Figure 10a–d show the SEM images of NiFe₂O₄/CHF at different magnifications. From the SEM images, we can observe that the NiFe₂O₄ nanoparticles are attached to the surface of the carbonized hemp fibers. Figure 10e–i show the element diagram and elemental mapping images of NiFe₂O₄/CHF in Figure 10d. It displays that the NiFe₂O₄/CHF is mainly composed of C, O, Fe, and Ni elements, and the Fe, Ni, and O elements are distributed along the NiFe₂O₄ nanoparticles on the carbonized hemp fibers. In addition, when the hemp fibers were changed to bamboo fibers under the same conditions, NiFe₂O₄ nanoparticles were also loaded on the carbonized bamboo fibers. Moreover, the microwave absorption performance of the NiFe₂O₄/carbonized bamboo fibers was also investigated (See Supporting Information Figure S5–S7). In general, the experimental results indicate that this facile self-assembly technology is universally applicable in designing other types of carbon matrix composites.

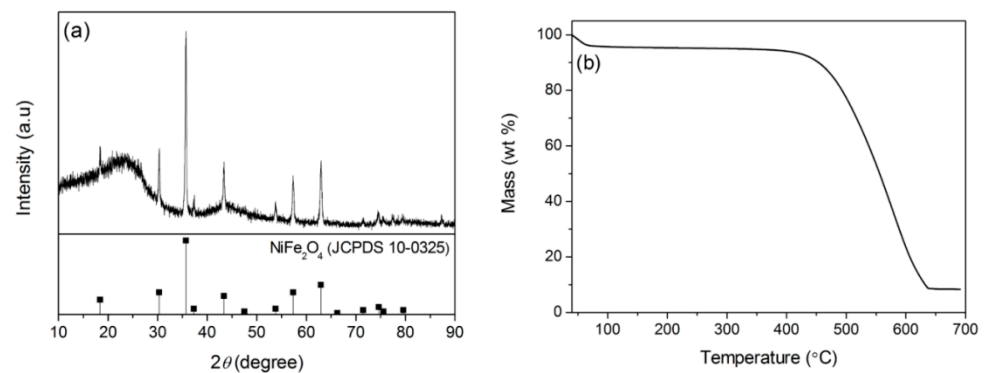


Figure 9. XRD pattern (a) and TG curve (b) of NiFe₂O₄/carbonized hemp fibers.

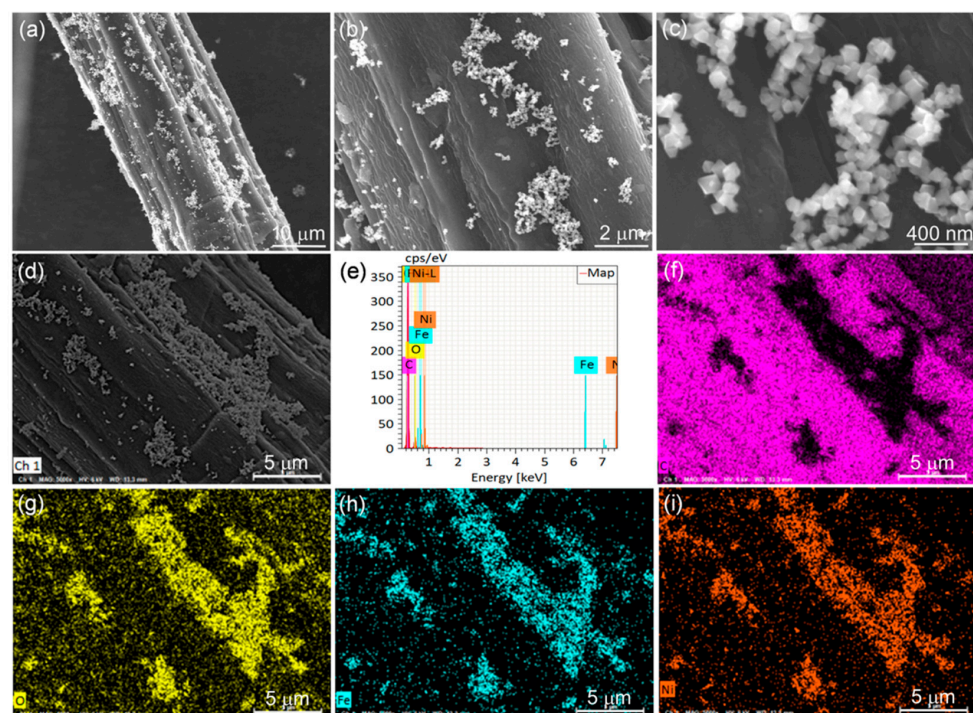


Figure 10. (a–d) SEM images, (e) EDX spectra, and (f–i) elemental mapping images of NiFe₂O₄/carbonized hemp fibers.

The electromagnetic properties of NiFe₂O₄/CHF dispersed in paraffin matrix with 33 wt % are shown in Figure 11. Figure 11a illustrates the complex permittivity of NiFe₂O₄/CHF. The ϵ' decreases from 9.4 to 5.5, and the ϵ'' is in the range of 2.1–2.6 with three vibration peaks. Figure 11b shows the complex permeability of NiFe₂O₄/CHF. Interestingly, the μ'' shows an opposite trend to ϵ'' , showing that there is an obvious electromagnetic synergistic effect, which is conducive to electromagnetic loss. Figure 11c displays the simulated RL curve of NiFe₂O₄/CHF at different thicknesses. The effective bandwidth is 5.85 GHz (12.15–18 GHz) with a minimum RL of -23.1 dB at a thickness of 2.0 mm. Figure 11d shows the impedance matching coefficient of NiFe₂O₄/CHF, which shows an upward trend in the frequency range 2–18 GHz, implying that the well-matched characteristic impedance contributes to high-frequency microwave absorption. Figure 11e illustrates the dielectric loss factor and magnetic loss factor. The curves of dielectric loss tangent and magnetic loss tangent are similar to ϵ'' and μ'' , respectively. This illustrates that the loss tangent is mainly affected by the imaginary part of the complex permittivity and permeability. Moreover, the dielectric and magnetic loss tangent present opposite vibration peaks, indicating a strong electromagnetic coupling effect [62]. In addition, the dielectric loss tangent gradually increases, which is in favor of high-frequency electromagnetic loss. Figure 11f corresponds to the Cole–Cole curve of NiFe₂O₄/CHF, which has three Cole–Cole semicircles, meaning that it has multiple relaxation processes and promoted interfacial polarization. Such polarization processes are conducive to dielectric loss. In a word, the impedance matching, and the synergy between dielectric loss and magnetic loss contribute to the enhanced microwave absorption performance of NiFe₂O₄/CHF.

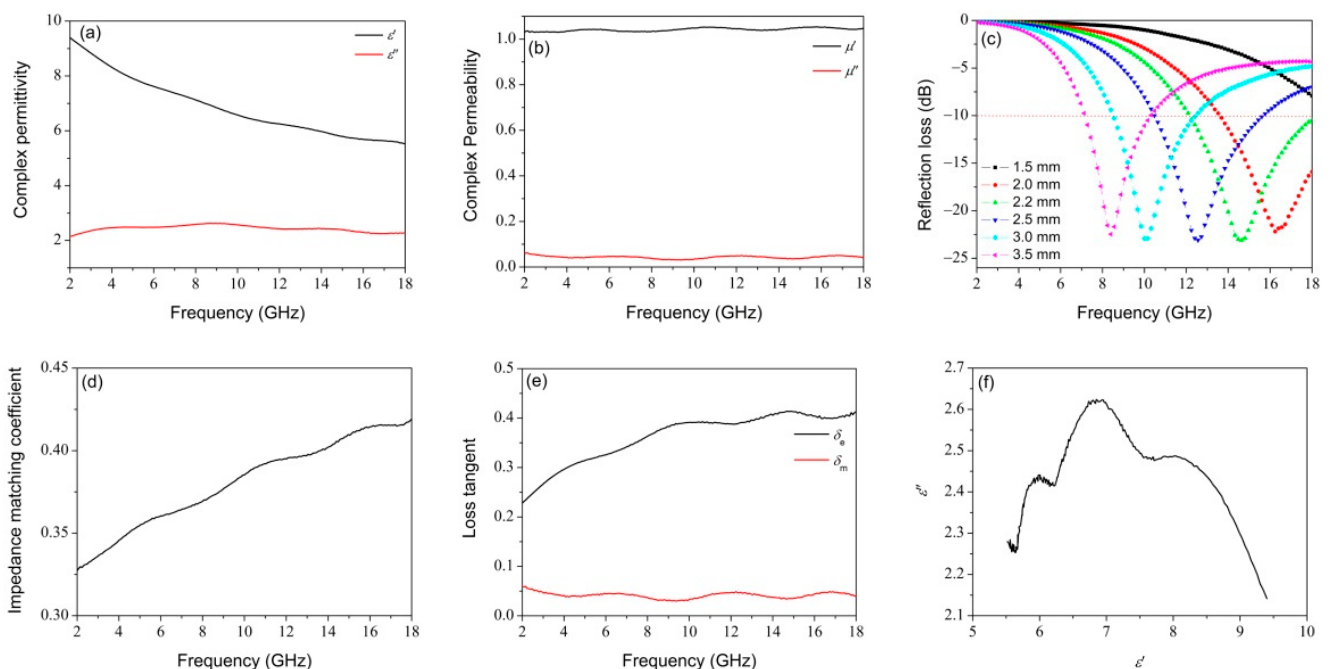


Figure 11. The frequency dependence of (a) complex permittivity, (b) complex permeability, (c) simulated reflection loss, (d) impedance matching coefficient, (e) loss factor, and (f) Cole–Cole curve of NiFe₂O₄/carbonized hemp fibers.

4. Discussion

To sum up, taking cotton fiber, hemp fiber, and bamboo fiber as the carbon source, the accurate loading of NiFe₂O₄ nanoparticles with different contents on biomass-based carbon fibers was successfully achieved. The results show that the impedance matching is optimized, and the microwave absorption performance is improved after loading NiFe₂O₄ nanoparticles on the biomass-based carbon fibers. In particular, when NiFe₂O₄ nanoparticles are loaded with 42.3 wt%, the effective bandwidth of the NiFe₂O₄/carbon

cotton fiber can reach 6.5 GHz with a minimum RL of -45.3 dB. The enhancement of microwave absorption performance is attributed to the appropriate loading amount of NiFe_2O_4 nanoparticles with moderate electromagnetic parameters, and the balance of impedance matching and electromagnetic loss. This study is expected to provide a new way for designing new carbon-based microwave-absorbing materials.

Supplementary Materials: The following supporting information can be downloaded at: <https://www.mdpi.com/article/10.3390/nano12224063/s1>, Figure S1: (a,b) TEM images of the NiFe_2O_4 nanoparticles in different magnification; Figure S2: Cole–Cole curves of (a) CCF, (b) NiFe_2O_4 /CCF-1, (c) NiFe_2O_4 /CCF-2, (d) NiFe_2O_4 /CCF-3, and (e) NiFe_2O_4 /CCF-4; Figure S3: Values of C_0 ($C_0 = \mu''\mu'^{-2}f^{-1}$) of CCF, NiFe_2O_4 /CCF-1, NiFe_2O_4 /CCF-2, NiFe_2O_4 /CCF-3, and NiFe_2O_4 /CCF-4; Figure S4: Simulation and calculation of the absorber thickness (t_m) versus peak frequency (f_m): (a) CCF, (b) NiFe_2O_4 /CCF-1, (c) NiFe_2O_4 /CCF-2, (d) NiFe_2O_4 /CCF-3, and (e) NiFe_2O_4 /CCF-4; Figure S5: XRD pattern of NiFe_2O_4 /carbonized bamboo fibers; Figure S6: (a–d) SEM images, (e) EDX spectra, and (f–i) elemental mapping images of NiFe_2O_4 /carbonized bamboo fibers; Figure S7: Frequency dependence of the simulated reflection loss for NiFe_2O_4 /carbonized bamboo fibers at different thicknesses.

Author Contributions: Conceptualization, methodology, formal analysis, writing—original draft, writing—review and editing, W.L.; investigation, resources, F.G.; visualization, data curation, Y.Z.; validation, Y.L. All authors have read and agreed to the published version of the manuscript.

Funding: This work was supported by the applied basic research project of Shanxi (No. 20210302124045), Shanxi province teaching reform and innovation project (No. J2021650), and Shanxi province collaborative innovation center for light materials modification and application.

Institutional Review Board Statement: Not applicable.

Informed Consent Statement: Not applicable.

Data Availability Statement: Not applicable.

Conflicts of Interest: The authors declare no conflict of interest.

References

1. Zeng, X.J.; Cheng, X.Y.; Yu, R.H.; Stucky, G.D. Electromagnetic microwave absorption theory and recent achievements in microwave absorbers. *Carbon* **2020**, *168*, 606–623. [CrossRef]
2. Wang, F.; Gu, W.H.; Chen, J.B.; Wu, Y.; Zhou, M.; Tang, S.L.; Cao, X.Z.; Zhang, P.; Ji, G.B. The point defect and electronic structure of K doped $\text{LaCo}_{0.9}\text{Fe}_{0.1}\text{O}_3$ perovskite with enhanced microwave absorbing ability. *Nano Res.* **2022**, *15*, 3720–3728. [CrossRef]
3. Zhang, M.; Cao, M.S.; Shu, J.C.; Cao, W.Q.; Li, L.; Yuan, J. Electromagnetic absorber converting radiation for multifunction. *Mater. Sci. Eng. R* **2021**, *145*, 100627. [CrossRef]
4. Zhang, Z.W.; Cai, Z.H.; Wang, Z.Y.; Peng, Y.L.; Xia, L.; Ma, S.P.; Yin, Z.Z.; Huang, Y. A review on metal–organic framework-derived porous carbon-based novel microwave absorption materials. *Nano-Micro Lett.* **2021**, *13*, 56. [CrossRef] [PubMed]
5. Zhao, Y.; Hao, L.L.; Zhang, X.D.; Tan, S.J.; Li, H.H.; Zheng, J.; Ji, G.B. A novel strategy in electromagnetic wave absorbing and shielding materials design: Multi-responsive field effect. *Small Sci.* **2022**, *2*, 2100077. [CrossRef]
6. Zhao, H.Q.; Cheng, Y.; Lv, H.L.; Ji, G.B.; Du, Y.W. A novel hierarchically porous magnetic carbon derived from biomass for strong lightweight microwave absorption. *Carbon* **2019**, *142*, 245–253. [CrossRef]
7. Duan, Y.B.; Liang, Q.X.; Yang, Z.; Li, Z.H.; Yin, H.Y.; Cao, Y.; Li, D.C. A wide-angle broadband electromagnetic absorbing metastructure using 3D printing technology. *Mater. Des.* **2021**, *208*, 109900. [CrossRef]
8. Yan, L.W.; Hong, C.Q.; Sun, B.Q.; Zhao, G.D.; Cheng, Y.H.; Dong, S.; Zhang, D.Y.; Zhang, X.H. In situ growth of core–sheath heterostructural SiC nanowire arrays on carbon fibers and enhanced electromagnetic wave absorption performance. *ACS Appl. Mater. Interfaces* **2017**, *9*, 6320–6331. [CrossRef]
9. He, X.; Peng, H.L.; Xiong, Z.Q.; Nie, X.L.; Wang, D.; Wang, G.S.; Liu, C.B. A sustainable and low-cost route to prepare magnetic particle-embedded ultra-thin carbon nanosheets with broadband microwave absorption from biowastes. *Carbon* **2022**, *198*, 195–206. [CrossRef]
10. Han, C.; Zhang, M.; Cao, W.Q.; Cao, M.S. Electrospinning and in-situ hierarchical thermal treatment to tailor C-NiCo₂O₄ nanofibers for tunable microwave absorption. *Carbon* **2021**, *171*, 953–962. [CrossRef]
11. Li, X.L.; Yin, X.W.; Song, C.Q.; Han, M.K.; Xu, H.L.; Duan, W.Y.; Cheng, L.F.; Zhang, L.T. Self-assembly core-shell graphene-bridged hollow MXenes spheres 3D foam with ultrahigh specific EM absorption performance. *Adv. Funct. Mater.* **2018**, *28*, 1803938. [CrossRef]

12. Jiang, Z.Y.; Si, H.X.; Chen, X.; Liu, H.M.; Zhang, L.; Zhang, Y.H.; Gong, C.H.; Zhang, J.W. Simultaneous enhancement of impedance matching and the absorption behavior of BN/RGO nanocomposites for efficiency microwave absorption. *Compos. Commun.* **2020**, *22*, 100503. [[CrossRef](#)]
13. Chen, X.T.; Zhou, M.; Zhao, Y.; Gu, W.H.; Wu, Y.; Tang, S.L.; Ji, G.B. Morphology control of eco-friendly chitosan-derived carbon aerogels for efficient microwave absorption at thin thickness and thermal stealth. *Green Chem.* **2022**, *24*, 5280–5290. [[CrossRef](#)]
14. Chen, C.; Xi, J.B.; Zhou, E.Z.; Peng, L.; Chen, Z.C.; Gao, C. Porous graphene microflowers for high-performance microwave absorption. *Nano-Micro Lett.* **2018**, *10*, 26. [[CrossRef](#)]
15. Guo, S.N.; Zhang, Y.Q.; Chen, J.B.; Wu, Y.; Cao, J.M.; Tang, S.L.; Ji, G.B. The excellent electromagnetic wave absorbing properties of carbon fiber composites: Effect of metal content. *Inorg. Chem. Front.* **2022**, *9*, 3244–3250. [[CrossRef](#)]
16. Zhang, X.C.; Zhang, X.; Yuan, H.R.; Li, K.Y.; Ouyang, Q.Y.; Zhu, C.L.; Zhang, S.; Chen, Y.J. CoNi nanoparticles encapsulated by nitrogen-doped carbon nanotube arrays on reduced graphene oxide sheets for electromagnetic wave absorption. *Chem. Eng. J.* **2020**, *383*, 123208. [[CrossRef](#)]
17. Wang, Y.C.; Yao, L.H.; Zheng, Q.; Cao, M.S. Graphene-wrapped multiloculated nickel ferrite: A highly efficient electromagnetic attenuation material for microwave absorbing and green shielding. *Nano Res.* **2022**, *15*, 6751–6760. [[CrossRef](#)]
18. Zhang, X.; Qiao, J.; Jiang, Y.Y.; Wang, F.L.; Tian, X.L.; Wang, Z.; Wu, L.L.; Liu, W.; Liu, J.R. Carbon-based MOF derivatives: Emerging efficient electromagnetic wave absorption agents. *Nano-Micro Lett.* **2021**, *13*, 135. [[CrossRef](#)]
19. Song, N.J.; Ma, C.L.; Li, P.; Li, W.X.; Guo, F.; Du, Y.E.; Chen, Y.Q. A novel method of enhancing the nitrogen content in biomass hard carbon: Pyrolysis-deposition-self-doping strategy. *Int. J. Energy Res.* **2022**, *46*, 9892–9899. [[CrossRef](#)]
20. Gu, W.H.; Sheng, J.Q.; Huang, Q.Q.; Wang, G.H.; Chen, J.B.; Ji, G.B. Environmentally friendly and multifunctional shaddock peel-based carbon aerogel for thermal insulation and microwave absorption. *Nano-Micro Lett.* **2021**, *13*, 102. [[CrossRef](#)]
21. Wu, N.N.; Liu, C.; Xu, D.M.; Liu, J.R.; Liu, W.; Shao, Q.; Guo, Z.H. Enhanced electromagnetic wave absorption of three-dimensional porous Fe₃O₄/C composite flowers. *ACS Sustain. Chem. Eng.* **2018**, *6*, 12471–12480. [[CrossRef](#)]
22. Shen, G.Z.; Ren, J.Z.; Zhao, B.; Mei, B.Q.; Wu, H.Y.; Fang, X.M.; Xu, Y.W. Magnetic hollow mesoporous carbon composites with impedance matching for highly effective microwave absorption. *J. Mater. Sci.* **2019**, *54*, 4024–4037. [[CrossRef](#)]
23. Wang, H.G.; Meng, F.B.; Li, J.Y.; Li, T.; Chen, Z.J.; Luo, H.B.; Zhou, Z.W. Carbonized design of hierarchical porous carbon/Fe₃O₄@Fe derived from loofah sponge to achieve tunable high-performance microwave absorption. *ACS Sustain. Chem. Eng.* **2018**, *6*, 11801–11810. [[CrossRef](#)]
24. Pinto, S.S.; Machado, J.P.B.; Gomes, N.A.S.; Rezende, M.C. Influence of the aspect ratio of magnetic metallic additives on the microwave absorbing performance. *Mater. Res. Express* **2017**, *4*, 096101. [[CrossRef](#)]
25. Gorriti, A.G.; Marin, P.; Cortina, D.; Hernando, A. Microwave attenuation with composite of copper microwires. *J. Magn. Magn. Mater.* **2010**, *322*, 1505–1510. [[CrossRef](#)]
26. Gueye, P.G.B.; Sánchez, J.L.; Navarro, E.; Serrano, A.; Marín, P. Control of the length of Fe_{73.5}Si_{13.5}Nb₃Cu₁B₉ microwires to be used for magnetic and microwave absorbing purposes. *ACS Appl. Mater. Interfaces* **2020**, *12*, 15644–15656. [[CrossRef](#)]
27. Li, W.X.; Qi, H.X.; Guo, F.; Du, Y.E.; Song, N.J.; Liu, Y.Y.; Chen, Y.Q. Co nanoparticles supported on cotton-based carbon fibers: A novel broadband microwave absorbent. *J. Alloys Compd.* **2019**, *772*, 760–769. [[CrossRef](#)]
28. Zhao, H.Q.; Cheng, Y.; Ma, J.N.; Zhang, Y.N.; Ji, G.B.; Du, Y.W. A sustainable route from biomass cotton to construct lightweight and high-performance microwave absorber. *Chem. Eng. J.* **2018**, *339*, 432–441. [[CrossRef](#)]
29. Wei, Y.; Liu, H.J.; Liu, S.C.; Zhang, M.M.; Shi, Y.P.; Zhang, J.W.; Zhang, L.; Gong, C.H. Waste cotton-derived magnetic porous carbon for high-efficiency microwave absorption. *Compos. Commun.* **2018**, *9*, 70–75. [[CrossRef](#)]
30. Yao, L.H.; Cao, W.Q.; Zhao, J.G.; Zheng, Q.; Wang, Y.C.; Jiang, S.; Pan, Q.L.; Song, J.; Zhu, Y.Q.; Cao, M.S. Regulating bifunctional flower-like NiFe₂O₄/graphene for green EMI shielding and lithium ion storage. *J. Mater. Sci. Eng.* **2022**, *127*, 48–60. [[CrossRef](#)]
31. Zhang, M.; Song, S.N.; Liu, Y.M.; Hou, Z.X.; Tang, W.Y.; Li, S.N. Microstructural design of necklace-like Fe₃O₄/multiwall carbon nanotube (MWCNT) composites with enhanced microwave absorption performance. *Materials* **2021**, *14*, 4783. [[CrossRef](#)] [[PubMed](#)]
32. Liu, J.L.; Zhang, L.M.; Wu, H.J. Enhancing the low/middle-frequency electromagnetic wave absorption of metal sulfides through F[−] regulation engineering. *Adv. Funct. Mater.* **2022**, *32*, 2110496. [[CrossRef](#)]
33. Liu, P.J.; Yao, Z.J.; Ng, V.M.H.; Zhou, J.T.; Kong, L.B.; Yue, K. Facile synthesis of ultrasmall Fe₃O₄ nanoparticles on MXenes for high microwave absorption performance. *Compos. Part A* **2018**, *115*, 371–382. [[CrossRef](#)]
34. Liang, X.H.; Quan, B.; Chen, J.B.; Gu, W.H.; Zhang, B.S.; Ji, G.B. Nano bimetallic@carbon layer on porous carbon nanofibers with multiple interfaces for microwave absorption applications. *ACS Appl. Nano Mater.* **2018**, *1*, 5712–5721. [[CrossRef](#)]
35. Zhang, R.N.; Qiao, J.; Zhang, X.; Yang, Y.F.; Zheng, S.N.; Li, B.; Liu, W.; Liu, J.R.; Zeng, Z.H. Biomass-derived porous carbon for microwave absorption. *Mater. Chem. Phys.* **2022**, *289*, 126437. [[CrossRef](#)]
36. Cheng, Y.; Ji, G.B.; Li, Z.Y.; Lv, H.L.; Liu, W.; Zhao, Y.; Cao, J.M.; Du, Y.W. Facile synthesis of FeCo alloys with excellent microwave absorption in the whole Ku-band: Effect of Fe/Co atomic ratio. *J. Alloys Compd.* **2017**, *704*, 289–295. [[CrossRef](#)]
37. Du, Y.C.; Liu, W.W.; Qing, R.; Wang, Y.; Han, X.J.; Ma, J.; Xu, P. Shell thickness-dependent microwave absorption of core-shell Fe₃O₄@C composites. *ACS Appl. Mater. Interfaces* **2014**, *6*, 12997–13006. [[CrossRef](#)] [[PubMed](#)]
38. Zhao, H.B.; Cheng, J.B.; Zhu, J.Y.; Wang, Y.Z. Ultralight CoNi/rGO aerogels toward excellent microwave absorption at ultrathin thickness. *J. Mater. Chem. C* **2019**, *7*, 441–448. [[CrossRef](#)]

39. Mu, Z.G.; Wei, G.K.; Zhang, H.; Gao, L.; Zhao, Y.; Tang, S.L.; Ji, G.B. The dielectric behavior and efficient microwave absorption of doped nanoscale LaMnO₃ at elevated temperature. *Nano Res.* **2022**, *15*, 7731–7741. [[CrossRef](#)]
40. Guan, X.M.; Yang, Z.H.; Zhu, Y.T.; Yang, L.J.; Zhou, M.; Wu, Y.; Yang, L.; Deng, T.W.; Ji, G.B. The controllable porous structure and s-doping of hollow carbon sphere synergistically act on the microwave attenuation. *Carbon* **2022**, *188*, 1–11. [[CrossRef](#)]
41. Liu, J.L.; Zhang, L.M.; Wu, H.J.; Zang, D.Y. Boosted electromagnetic wave absorption performance from vacancies, defects and interfaces engineering in Co(OH)F/Zn_{0.76}Co_{0.24}S/Co₃S₄ composite. *Chem. Eng. J.* **2021**, *411*, 128601. [[CrossRef](#)]
42. Masoudpanah, S.M. PVP-assisted hydrothermal synthesis of rod-like NiCo₂O₄ powders as high-performance microwave absorbers. *J. Mater. Res. Technol.* **2022**, *20*, 3264–3274. [[CrossRef](#)]
43. Cai, L.; Pan, F.; Zhu, X.J.; Dong, Y.Y.; Shi, Y.Y.; Xiang, Z.; Cheng, J.; Jiang, H.J.; Shi, Z.; Lu, W. Etching engineering and electrostatic self-assembly of N-doped MXene/hollow Co-ZIF hybrids for high-performance microwave absorbers. *Chem. Eur. J.* **2022**, *434*, 133865. [[CrossRef](#)]
44. Deng, L.J.; Han, M.G. Microwave absorbing performances of multiwalled carbon nanotube composites with negative permeability. *Appl. Phys. Lett.* **2007**, *91*, 023119. [[CrossRef](#)]
45. Liu, P.J.; Ng, V.M.H.; Yao, Z.J.; Zhou, J.T.; Lei, Y.M.; Yang, Z.H.; Lv, H.L.; Kong, L.B. Facile synthesis and hierarchical assembly of flowerlike NiO structures with enhanced dielectric and microwave absorption properties. *ACS Appl. Mater. Interfaces* **2017**, *9*, 16404–16416. [[CrossRef](#)]
46. Lü, Y.Y.; Wang, Y.T.; Li, H.L.; Lin, Y.; Jiang, Z.Y.; Xie, Z.X.; Kuang, Q.; Zheng, L.S. MOF-derived porous Co/C nanocomposites with excellent electromagnetic wave absorption properties. *ACS Appl. Mater. Interfaces* **2015**, *7*, 13604–13611. [[CrossRef](#)]
47. Yan, F.; Guo, D.; Zhang, S.; Li, C.Y.; Zhu, C.L.; Zhang, X.T.; Chen, Y.J. An ultra-small NiFe₂O₄ hollow particle/graphene hybrid: Fabrication and electromagnetic wave absorption property. *Nanoscale* **2018**, *10*, 2697–2703. [[CrossRef](#)]
48. Wang, L.X.; Guan, Y.K.; Qiu, X.; Zhu, H.L.; Pan, S.B.; Yu, M.X.; Zhang, Q.T. Efficient ferrite/Co/porous carbon microwave absorbing material based on ferrite@metal–organic framework. *Chem. Eng. J.* **2017**, *326*, 945–955. [[CrossRef](#)]
49. Li, X.; Cui, E.B.; Xiang, Z.; Yu, L.Z.; Xiong, J.; Pan, F.; Lu, W. Fe@NPC@CF nanocomposites derived from Fe-MOFs/biomass cotton for lightweight and high-performance electromagnetic wave absorption applications. *J. Alloys Compd.* **2020**, *819*, 152952. [[CrossRef](#)]
50. Yan, J.; Huang, Y.; Chen, X.F.; Wei, C. Conducting polymers-NiFe₂O₄ coated on reduced graphene oxide sheets as electromagnetic (EM) wave absorption materials. *Synth. Metals* **2016**, *221*, 291–298. [[CrossRef](#)]
51. Xie, P.T.; Li, H.Y.; He, B.; Dang, F.; Lin, J.; Fan, R.H.; Hou, C.X.; Liu, H.; Zhang, J.X.; Ma, Y.; et al. Bio-gel derived nickel/carbon nanocomposites with enhanced microwave absorption. *J. Mater. Chem. C* **2018**, *6*, 8812–8822. [[CrossRef](#)]
52. Shen, Z.J.; Yang, H.L.; Xiong, Z.Q.; Xie, Y.; Liu, C.B. Hollow core-shell CoNi@C and CoNi@NC composites as high-performance microwave absorbers. *J. Alloys Compd.* **2021**, *871*, 159574. [[CrossRef](#)]
53. Wang, S.S.; Zhao, Y.; Xue, H.L.; Xie, J.R.; Feng, C.H.; Li, H.S.; Shi, D.X.; Muhammad, S.; Jiao, Q.Z. Preparation of flower-like CoFe₂O₄@graphene composites and their microwave absorbing properties. *Mater. Lett.* **2018**, *223*, 186–189. [[CrossRef](#)]
54. Ojha, G.P.; Pant, B.; Acharya, J.; Park, M. An electrochemically reduced ultra-high mass loading three-dimensional carbon nanofiber network: A high energy density symmetric supercapacitor with a reproducible and stable cell voltage of 2.0 V. *Nanoscale* **2021**, *13*, 19537–19548. [[CrossRef](#)] [[PubMed](#)]
55. Liu, W.; Tan, S.J.; Yang, Z.H.; Ji, G.B. Enhanced low frequency electromagnetic properties of MOF-derived cobalt through interface design. *ACS Appl. Mater. Interfaces* **2018**, *10*, 31610–31622. [[CrossRef](#)]
56. Ding, D.; Wang, Y.; Li, X.D.; Qiang, R.; Xu, P.; Chu, W.L.; Han, X.J.; Du, Y.C. Rational design of core shell Co@C microspheres for high performance microwave absorption. *Carbon* **2017**, *111*, 722–732. [[CrossRef](#)]
57. Pan, H.X.; Yin, X.W.; Xue, J.M.; Cheng, L.F.; Zhang, L.T. In-situ synthesis of hierarchically porous and polycrystalline carbon nanowires with excellent microwave absorption performance. *Carbon* **2016**, *107*, 36–45. [[CrossRef](#)]
58. Wang, S.S.; Jiao, Q.Z.; Liu, X.F.; Xu, Y.C.; Shi, Q.; Yue, S.; Zhao, Y.; Liu, H.B.; Feng, C.H.; Shi, D.X. Controllable synthesis of γ -Fe₂O₃ nanotube/porous rGO composites and their enhanced microwave absorption properties. *ACS Sustain. Chem. Eng.* **2019**, *7*, 7004–7013. [[CrossRef](#)]
59. Huang, W.H.; Wang, S.; Yang, X.F.; Zhang, X.X.; Zhang, Y.N.; Pei, K.; Che, R.C. Temperature induced transformation of Co@C nanoparticle in 3D hierarchical core-shell nanofiber network for enhanced electromagnetic wave adsorption. *Carbon* **2022**, *195*, 44–56. [[CrossRef](#)]
60. Kang, Y.; Jiang, Z.H.; Ma, T.; Chu, Z.Y.; Li, G.Y. Hybrids of reduced graphene oxide and hexagonal boron nitride: Lightweight absorbers with tunable and highly efficient microwave attenuation properties. *ACS Appl. Mater. Interfaces* **2016**, *8*, 32468–32476. [[CrossRef](#)]
61. Fang, G.; Liu, C.Y.; Yang, Y.; Peng, K.S.; Cao, Y.F.; Jiang, T.; Zhang, Y.T.; Zhang, Y.J. Regulating percolation threshold via dual conductive phases for high-efficiency microwave absorption performance in C and X bands. *ACS Appl. Mater. Interfaces* **2021**, *13*, 37517–37526. [[CrossRef](#)] [[PubMed](#)]
62. Wang, K.F.; Chen, Y.J.; Tian, R.; Li, H.; Zhou, Y.; Duan, H.N.; Liu, H.Z. Porous Co-C core-shell nanocomposites derived from Co-MOF-74 with enhanced electromagnetic wave absorption performance. *ACS Appl. Mater. Interfaces* **2018**, *10*, 11333–11342. [[CrossRef](#)] [[PubMed](#)]